

This is the accepted manuscript made available via CHORUS. The article has been published as:

G^{\prime} band in double- and triple-walled carbon nanotubes: A Raman study

Thomas Ch. Hirschmann, Mildred S. Dresselhaus, Hiroyuki Muramatsu, Max Seifert,
Ursula Wurstbauer, Eric Parzinger, Kornelius Nielsch, Yoong Ahm Kim, and Paulo T. Araujo

Phys. Rev. B **91**, 075402 — Published 2 February 2015

DOI: [10.1103/PhysRevB.91.075402](https://doi.org/10.1103/PhysRevB.91.075402)

G'-Band in Double- and Triple-Walled Carbon Nanotubes: A Raman Study

Thomas Ch. Hirschmann,^{#,+,*} Mildred S. Dresselhaus,^{+,∞,*} Hiroyuki Muramatsu,[§] Max Seifert,[‡] Ursula Wurstbauer,[‡] Eric Parzinger,[‡] Kornelius Nielsch,[#] Yoong Ahm Kim,^{§,‡} and Paulo T. Araujo,^{‡,*}

[#]*Institute of Applied Physics, University of Hamburg, 20355 Hamburg, Germany.*

⁺*Department of Electrical Engineering and Computer Science and [∞]Department of Physics, Massachusetts Institute of Technology, Cambridge, Massachusetts 02139-4307, United States*

[§]*Faculty of Engineering, Shinshu University, 4-17-1 Wakasato, Nagano 380-8553, Japan*

[‡]*Walter Schottky Institut and Physik Department,*

Technische Universität München, 85748 Garching, Germany

[‡]*Polymer and Fiber System Engineering, Chonnam National University, 77 Yongbong-ro, buk-gu, Gwangju 500-757, Korea*

[‡]*Department of Physics and Astronomy, University of Alabama, Tuscaloosa, Alabama 35401, United States*
*Email: *thirschm@physnet.uni-hamburg.de; *millie@mgm.mit.edu; *paulo.t.araujo@ua.edu*

Double- and triple-walled carbon nanotubes are studied in detail by laser energy dependent Raman spectroscopy in order to get a deeper understanding about the second order G'-band Raman process, general nanotube properties, such as electronic and vibrational properties, and the growth method itself. In this work, the inner nanotubes from the double- and triple-walled carbon nanotubes are produced through the encapsulation of fullerene-peapods with high-temperature thermal treatments. We find that the spectral features of the G'-band, such as the intensity, frequency, line width, and line shape are highly sensitive to the annealing temperature variations. We also discuss the triple-peak structure of the G'-band observed in an individual triple-walled carbon nanotube taken at several laser energies connecting its Raman spectra with that for the G'-band spectra obtained for bundled triple-walled carbon nanotubes.

I. INTRODUCTION

A double-walled carbon nanotube (DWNT) is a system of two weakly-coupled concentric single-walled carbon nanotubes (SWNTs) separated by a certain wall-to-wall (WtW) distance.^{1,2} Each concentric nanotube can be either semiconducting (S) or metallic (M) so that a DWNT can have four different DWNT flavors (inner@outer nanotube), namely S@S, M@M, S@M, and M@S. Triple-walled carbon nanotubes (TWNTs) are ideal for studying the intertube interactions occurring for these DWNT flavors because the outer concentric nanotube shields the two inner nanotubes from external environmental influences. A better understanding of the electronic and vibrational properties of these few-walled carbon nanotubes (FWNTs) leads to a higher potential for novel technological applications in the fields of mechanics, electronics, thermal physics, bio-physics and many others. To characterize our DWNTs and TWNTs we used resonant Raman spectroscopy (RRS), which has been shown to provide a strategic technique for studying carbon-based materials³, since RRS is a fast and non-destructive technique. Our recent RRS studies on DWNTs and TWNTs advanced the understanding of both the mechanisms behind the growth methods and their optical properties.^{1,2} The Raman spectra of carbon nanotubes distinctly show several different carbon vibrational modes.³

An important Raman mode is the coherent motion of the carbon atoms in the radial direction, called the radial breathing mode (RBM). This first-order Raman

scattering process is unique for each nanotube and is the ultimate confirmation of the existence of nanotubes in a given sample. Its frequency of vibration (ω_{RBM}) is inversely proportional⁴ to the nanotube diameter (d_t) and ω_{RBM} can usually be found below 400 cm^{-1} . Another important Raman feature of nanotubes is the G-band, which is also a first-order Raman scattering process observed at around 1600 cm^{-1} . The G-band is composed of two main components, the tangential optical (TO) mode and the longitudinal optical (LO) mode, also denoted by G^- and G^+ .⁵ The defect-induced band (D-band) of a carbon nanotube is often a weak Raman feature compared to the other most relevant Raman modes and gives information about the structural quality of the carbon nanotubes under investigation.⁶ This Raman mode is due to a double resonant Raman scattering process which involves one-phonon scattering event and one elastic scattering event arising from an imperfection in the material. The D-band frequency (ω_D) is located in the range of 1300–1400 cm^{-1} . The overtone mode related to the D-band is the historically named the G'-band. It is worth mentioning that in the past the G'-band has also been named the D*-band or 2D-band.^{7,8} The G'-band frequency ($\omega_{G'}$) is located in the high frequency region at around 2700 cm^{-1} . The G' vibrational mode originates from a double resonant Raman scattering process where a two-phonon scattering mechanism is involved and this Raman mode is independent of structural defects.³ This double-resonant Raman process enables a careful study of wave vector-dependent phonon features and this G'-band is a good example, where the phonon frequency shows a clear Raman

dispersive behavior⁹ which is observed by changing the laser excitation energy (E_{laser}). Historically, the G'-band has been explored in many different ways to gain a comprehensive insight into both electronic and vibrational behaviors in: graphite⁹, mono-, bi- and multilayer graphene¹⁰, stacking order between the layers of graphene^{11,12}, SWNTs¹³, and environment influences on carbon nanotubes, for example, pressure or tension¹⁴⁻¹⁶. The G'-band frequency of carbon nanotubes is not only dependent on the E_{laser} but also on the nanotube diameter.¹⁷⁻²¹ In 2005, Pfeiffer *et al.*²² studied in detail for the first time such dependences of the G'-band of bundled DWNTs. Here, the G'-band showed a clear two-peak structure due to the diameter differences between the inner and the outer nanotubes. The $\omega_{G'}$ dependence with d_t becomes more evident when high hydrostatic pressures are applied to DWNTs showing that the $\omega_{G'}$ upshifts by increasing the external pressure. Namely, the G'-band for the outer nanotubes shifted by 16.7 cm⁻¹/GPa, while the G'-band for the inner nanotubes changes by 7.3 cm⁻¹/GPa when applying external pressure to the system under investigation.²³ Very recently, Alencar *et al.*²⁴ published a Raman study on a peapod-derived nanotube sample including DWNTs and TWNTs, where hydrostatic pressure was utilized to successfully identify the two distinct FWNTs by analyzing the pressure-dependence of the RBM frequencies. Indeed, using external pressure provides a useful method to analyze samples containing several kinds of nanotubes in a FWNT sample. In addition to the above mentioned frequency shifts, the G'-band intensities are clearly different for metallic nanotubes in comparison to semiconducting nanotubes (metallicity dependence).²⁵ Moreover, the intensities from the G'-band increase for small nanotube diameters ($d_t < 1$ nm), due to enhancements related to diameter-dependent electron-phonon coupling mechanisms.²⁶ The inner nanotubes of peapod-derived FWNTs have nanotube diameters around 0.7 nm and thus, they are ideal candidates to study electronic and vibrational properties of small diameter and high-curvature nanotubes. Also, a G'-band study on peapod-derived DWNTs where the inner nanotubes were grown by ¹³C-enriched carbon, showed an anomalous G'-band Raman dispersion for the inner nanotubes due to a curvature-induced and wavevector-dependent phonon energy softening.²⁷

In this paper, we present a detailed study of the G'-band of DWNTs and TWNTs, where the inner nanotubes were produced through a high-temperature heat treatment of the fullerene-peapods inside of their host nanotubes.^{28,29} By changing the annealing temperature, we clearly observe modifications in the RBM and G'-band spectra of the bundled DWNTs. Changing the diameter range of the concentric nanotubes results in a variation of the dominant flavors of the nanotubes that are in resonance with given laser excitation energies. For different types of nanotubes, important spectral

changes in intensity, frequency, line width, and line shape are observed. The G'-band of bundled carbon nanotubes with a given nanotube diameter distribution is relatively broad so that an accurate (n,m) index assignment is demanding. Raman studies of individual species would circumvent such assignment problems, but so far significant $\omega_{G'}$ results from individual DWNTs are scarce, and results for individual TWNTs are to the best of the authors knowledge non-existent. We here report detailed results on the G'-band of an individual TWNT, where each concentric nanotube contributes independently to the G'-band, and due to the nanotube diameter differences, we observe three well resolved G'-peaks. By changing the laser excitation energy, we are able to study the frequency, width and intensity variations of this triple-peak structure and we can analyze the G'-band from bundled TWNTs in a more systematic and precise way. The results presented here for DWNTs and TWNTs shed new light on the general understanding of the G'-band in FWNT systems.

II. EXPERIMENTAL DETAILS

The starting material used to fabricate the peapod-derived DWNTs was high-quality SWNTs produced by the arc-discharge method.²⁸ The nanotube diameters of these SWNTs were larger than 1.2 nm, allowing us to fill these SWNTs (host nanotubes) with fullerenes under vacuum conditions. After we removed the residual fullerenes attached to the outer part of the host nanotubes, we transformed the aligned fullerene-peapods into inner nanotubes for the DWNT systems^{30,31} by applying a high-temperature thermal treatment between 1500 and 2000 °C. Using these high annealing temperatures in an argon atmosphere, we were also able to increase the DWNT quality by annealing out structural defects.²⁸ Two Raman setups equipped with laser excitation sources $E_{\text{laser}} = 1.96$ and 2.41 eV and with a spectral resolutions of less than 0.5 and 0.6 cm⁻¹, respectively, were utilized to characterize the DWNT samples.

The TWNTs were produced using the same peapod method as described above, but instead of SWNTs as a host material, we used diameter-enlarged catalytic chemical vapor deposition (CVD) grown DWNTs. We encapsulated the fullerenes at an annealing temperature of 2000 °C to create high-quality TWNTs.²⁹ Individual TWNTs were placed on top of a silicon Si/SiO₂ substrate marked with a small gold grid (square sizes up to 12 × 12 μm) by spin-coating a solution containing individual TWNTs. These procedures allowed repeated access to some individual TWNTs on the substrate.¹ The Raman spectra of the bundled and individual TWNTs were taken using a Raman setup which includes an argon ion laser and a tunable rhodamine dye laser with several laser lines, providing us with energies between 2.10 and

2.54 eV. Additional and relevant spectral information about the RBMs, D-band and G-band for individual and bundled TWNTs have been recently reported.^{1,2}

III. RESULTS

A. Bundled Double-Walled Carbon Nanotubes

Figure 1 shows the Raman spectra taken at (a) $E_{\text{laser}} = 1.96$ eV and (b) 2.41 eV for the host SWNTs, as well as for the resulting DWNTs after annealing the fullerenes at temperatures ranging from 1500 to 2000 °C. The Raman intensities of all spectra are normalized in the low frequency range to the strongest RBM intensity of the host nanotubes and in the high frequency range to the strongest G' -band intensity. The low Raman frequency range for both E_{laser} lines yields RBM features for the host SWNTs between 148–189 cm^{-1} at 1.96 eV and between 152–181 cm^{-1} at 2.41 eV. These ω_{RBM} frequencies for the host nanotube correspond to SWNT diameters in the range from 1.26 to 1.65 nm using the relation³²

$$\omega_{\text{RBM}} = \frac{218.3}{d_t} + 15.9. \quad (1)$$

This relation can be transformed with the following equation³³

$$\omega_{\text{RBM}} = \frac{227}{d_t} \sqrt{1 + C_e \cdot d_t^2}, \quad (2)$$

in which C_e is 0.065. We use this relation to determine the nanotube diameters from all bundled samples, since this relation describes well nanotubes under environmental influences in the relevant RBM frequency range. The single and relatively broad peak, centered at 2629 cm^{-1} for $E_{\text{laser}} = 1.96$ eV and at 2680 cm^{-1} for $E_{\text{laser}} = 2.41$ eV, reflects the G' -band of the host SWNTs (G'_{host}). We notice in Fig. 1 that the ω_{RBM} values for the host SWNTs taken at two distinct E_{laser} are located around the same frequencies, and the G' -band shows a clear E_{laser} dependency. The Raman spectra for the DWNTs show, in addition to the host nanotube responses, both RBM peaks at higher ω_{RBM} values and a second additional G' -band feature (G'_{inner}) at lower $\omega_{G'}$ coming from the inner nanotubes. At this point it is important to remember that the RBMs of the inner nanotubes from bundled DWNTs consist of clusters of narrow peaks in comparison to the single-peak characteristics of bundled SWNTs.³⁴ Several Raman studies have discussed the G' -bands of bundled DWNTs, for example, the frequency shifts and intensity changes associated with the $\omega_{G'}$ dependence on E_{laser} , as well as on the growth method or the amount of dopants.^{22,35–39} The present work brings out a new discussion of the annealing temperature dependence of the G' -band for DWNTs.

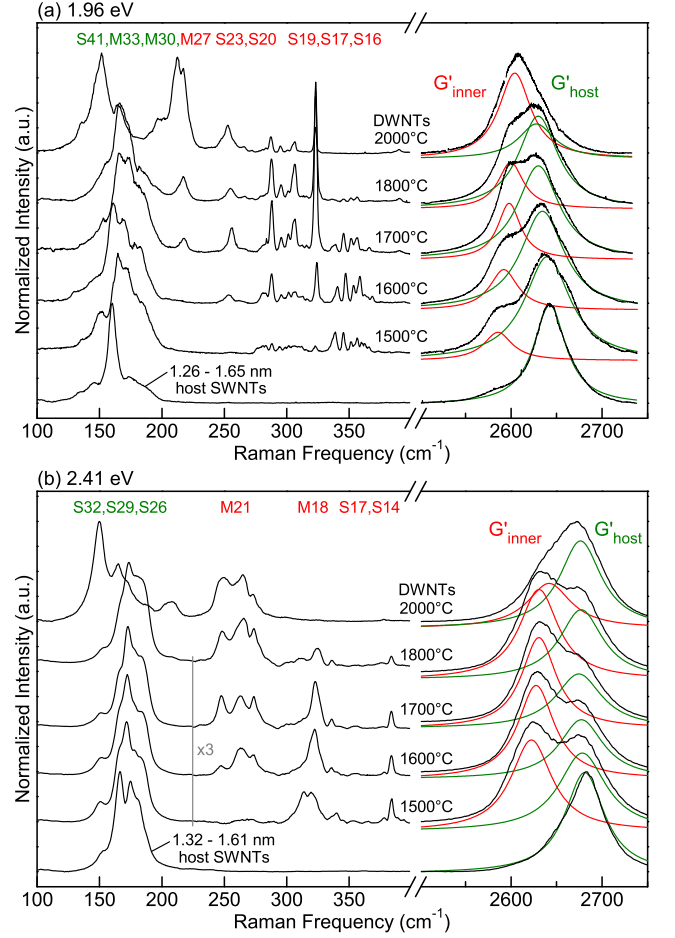


FIG. 1. The Raman spectra represent RBM (low frequency range) and G' -band (high frequency range) features of the host SWNTs (bottom spectrum) together with the corresponding spectra for the bundled DWNTs (other spectra), where the nanotubes are annealed at various temperatures between 1500 and 2000 °C taken with E_{laser} lines of (a) 1.96 eV and (b) 2.41 eV. The identification of peaks with specific spectral features are the host nanotubes which have ω_{RBM} below 225 cm^{-1} and for the inner nanotubes ω_{RBM} , which are between 225 and 400 cm^{-1} . The RBM regions of resonant ($2n+m$) families are indicated by green (host nanotubes) and red (inner nanotubes) color identifications. The G' -band features occur above 2550 cm^{-1} for the inner and host nanotubes.

Changes in the annealing temperature have an impact on the nanotube diameter distribution as well as on the intertube interactions, and this is reflected in the RBM frequency shifts and hence also in the details of the second order Raman scattering process in the high Raman frequency range above 2550 cm^{-1} . The RBM intensities for the inner nanotubes annealed at 1500 °C and shown in Fig. 1 are observed between 275 and 400 cm^{-1} , and come from inner nanotubes with diameters smaller than 0.85 nm. The D-band of the bundled DWNTs annealed at 1500 °C showed²⁸ relative strong intensities in comparison to the bundled DWNTs

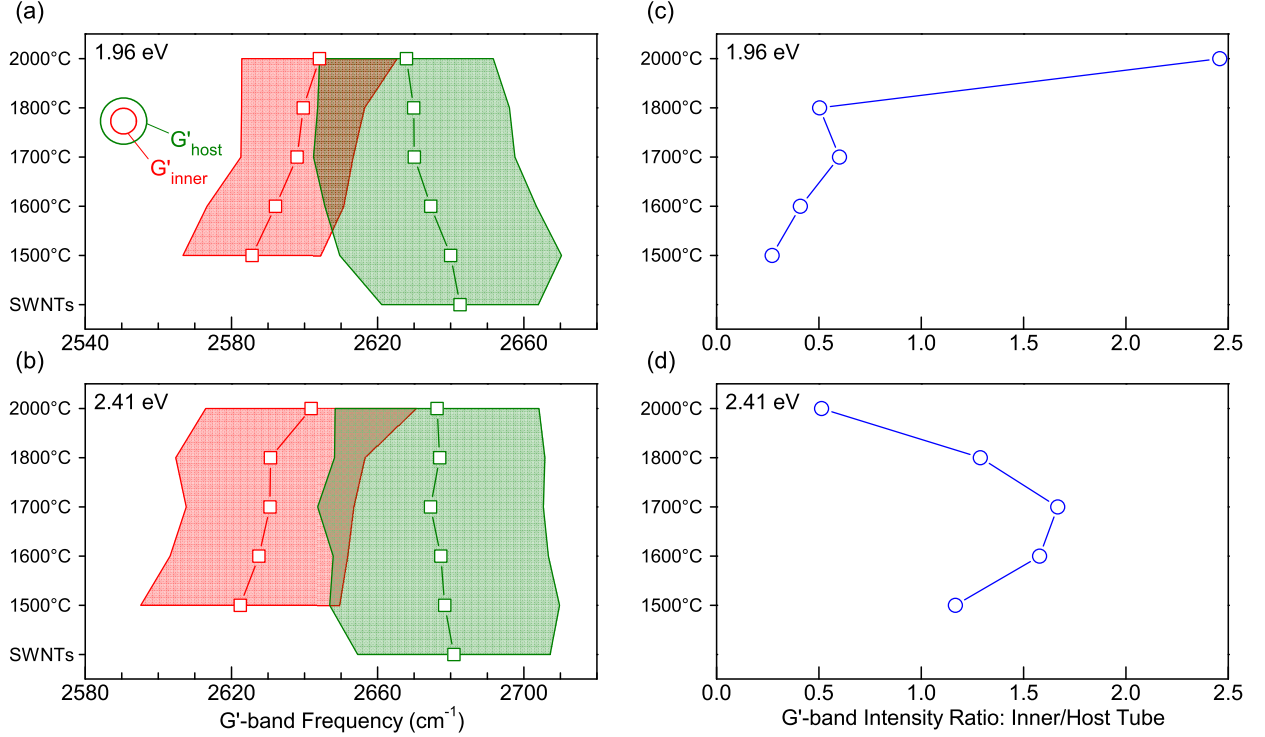


FIG. 2. The peak frequencies of the G'-band for the inner and the host nanotubes (a,b), and the peak intensity ratios (c,d) of the G'-bands for both the inner and host nanotubes are plotted as a function of annealing temperature. The host nanotubes in this figure are the outer nanotubes of the DWNT bundles. The error bars represent the fwhm of the peaks for the Raman spectra taken at 1.96 eV (a) and at 2.41 eV (b). The G'-band at the lower frequency belongs to the inner nanotubes (G'_{inner} and as indicated in the schematic cross sectional view), and by increasing the annealing temperature this peak shifts towards higher frequencies, and hence to larger inner nanotube diameters. This tendency is also reflected through the RBM spectra shown in Fig. 1.

heat treated at temperatures higher than 1600 °C. This observation together with the Raman spectrum at 1500 °C in Fig. 1 indicate that the fullerenes just merged to each other but that the inner nanotubes are not completely formed yet. The RBM intensity distribution of the inner nanotubes peaks shift towards lower frequencies every time the annealing temperature increases from 1500 °C up to 1800 °C. This tendency explains that higher annealing temperatures produce inner nanotube with larger diameters. When the thermal annealing temperature reaches 2000 °C both the host and the inner nanotube RBM frequencies shift toward lower frequencies and DWNTs with enlarged nanotube diameters are produced. This conclusion is in fact reasonable because at temperatures of 1800 °C and below, we are already close to the Debye temperature for fullerenes. As a consequence, they start coalescing to form inner nanotubes with several diameters. However, at temperatures around 2000 °C the nanotube system is already close enough to the Debye temperature of carbon nanotubes, which might favors the coalescence of adjacent DWNT species. High-resolution transmission electron microscopy (TEM) studies confirmed that this DWNT formation process can occur²⁸, and that

at certain temperatures (depending on the system), the coalescence of adjacent nanotubes occurs.^{40–43} Using our previous analysis described in Ref. 1, we determine in Fig. 1 the most likely resonant nanotube families ($2n+m = \text{constant number}$) contained in our samples. We see that, at low annealing temperatures, for example, the DWNT spectra are dominated by the S@M flavor for $E_{\text{laser}} = 1.96$ eV, while it is the M@S flavor for $E_{\text{laser}} = 2.41$ eV. These flavor differences are also reflected in the G'-band peak intensities and in the G'-peak intensity ratios for the inner/host nanotubes ($I_{\text{inner}}^{G'}/I_{\text{host}}^{G'}$), where the metallic nanotubes contribute more strongly to the respective frequency parts of the G'-band intensities. It is important to comment, however, that other DWNT flavors are also in resonant with the presented E_{laser} , as, for example, the M@S and M@M flavors at an annealing temperature of 2000 °C at $E_{\text{laser}} = 1.96$ eV. Our previous study² on these DWNT samples discussed various intertube interaction dependencies, identified by the ω_{RBM} behaviors of the inner fullerene-peapod-derived nanotubes. In detail, by changing the annealing temperature, we observed that the intertube interactions in peapod-derived DWNTs decrease every time the annealing temperature is increased.

The $\omega_{G'}$ positions for both the inner nanotubes (red color) and the host nanotubes (green color) are plotted for $E_{\text{laser}} = 1.96$ eV in Fig. 2(a), and for $E_{\text{laser}} = 2.41$ eV in Fig. 2(b). The error bars represent the full width at half-maximum (fwhm) intensity of the Lorentzian-fits to the Raman modes. Figures 2(c,d) show the intensity ratios $I_{\text{inner}}^{G'}/I_{\text{host}}^{G'}$ for the inner/host nanotubes. This representation of the G' -band analysis uncovers the following observations: We notice, that the G' -peak widths at 1.96 eV are narrower and the G' -peak positions are closer together compared to the positions and widths at 2.41 eV. Moreover, by increasing the annealing temperature, the G' -band frequencies of the inner nanotubes explicitly upshift, while the fwhm line widths overlap more strongly at higher annealing temperatures for both laser excitation energies. This is in remarkably good agreement with the RBM intensities, demonstrating that lower annealing temperatures are sufficient to anneal the small diameter inner nanotubes, while higher temperatures are necessary to anneal the larger diameter inner nanotubes. The apparent frequency downshift of the G' -band for the host nanotubes can be explained by a close look at the RBM spectra of the host nanotubes in Fig. 1. Here, we mention the intensity differences of the features on the shoulders with increasing frequencies so that the G' -peak intensity behaviors reported in Figs. 2(c,d) are obtained.

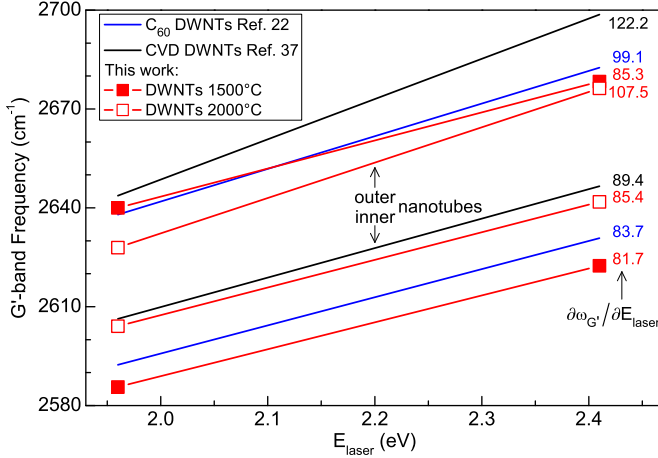


FIG. 3. The E_{laser} vs. $\omega_{G'}$ relations of the inner (lower four relations) and the outer (upper four relations) nanotube from bundled DWNTs are presented. The blue and black lines are, respectively, the fitted linear relations for fullerene-peapod derived DWNTs²² and for CVD DWNTs³⁷. The red lines are adapted from the Raman results for the bundled DWNTs produced with 1500 and 2000 °C, and depicted in Fig. 1. Differences in the growth methods are directly reflected in a change of the G' -band dispersions.

Looking at the peak intensity ratio $I_{\text{inner}}^{G'}/I_{\text{host}}^{G'}$ at 1.96 eV in Fig. 2(c), we observe how the G'_{inner} -band intensity increases slightly with annealing temperature, and this

behavior originates from the appearances of the RBM intensity of the metallic inner nanotubes likely from the M27 family. A strong increase in the $I_{\text{inner}}^{G'}$ from the 1800 to 2000 °C samples confirms that the DWNT diameter enlargement, the dominance of the M27 inner nanotubes in the RBM spectrum at 2000 °C, and the dominated DWNT flavor changes from S@M at 1800 °C to M@S at 2000 °C. On the other hand, the behavior of the peak intensity at $E_{\text{laser}} = 2.41$ eV in Fig. 2(d) regarding its dependency on the annealing temperature is denoted by sensitive changes of the metallic inner nanotubes. In this connection the G' -band change from 1800 to 2000 °C in Fig. 2(b) shows both, a frequency upshift of the inner G' -peak position and a wide overlap of the G' -band widths. This finding tells us how strongly the M18 family contributes to the observed G' -band intensity, and this is confirmed by the facts that the intensity ratio $I_{\text{inner}}^{G'}/I_{\text{host}}^{G'}$ decreases greatly by increasing the annealing temperature from 1800 to 2000 °C. The intensities of the RBMs of the M18 family are weak, meaning that the observed diameter enlargement of both the host and the inner nanotubes are shifting the resonance frequency of those metallic species in family M18 away from E_{laser} . The spectral changes of the G' -band intensities in combination with the RBM intensities provide clear evidence that the G' -band intensity of the carbon nanotube has a diameter as well as a metallicity dependence.

Figure 3 depicts the nanotube diameter dependence on the G' -band frequencies. Here, the linear fit relations of the inner and outer nanotubes from four different bundled DWNT systems are plotted and each $\partial\omega_{G'}/\partial E_{\text{laser}}$ dispersion is labeled on the right side. The G' -band dispersion generated with the two laser energies for the inner nanotube from bundled DWNTs produced with 1500 and 2000 °C are: $\partial\omega_{G'}/\partial E_{\text{laser}} = 81.7$ cm⁻¹/eV and $\partial\omega_{G'}/\partial E_{\text{laser}} = 85.4$ cm⁻¹/eV. Such G' -band dependencies on E_{laser} are expected for this double-resonance Raman feature.^{22,37} We observe similarities in the dispersions of the G' -bands and we note that the inner nanotubes show a clear frequency difference due to nanotube diameter differences.

B. Individual and Bundled Triple-Walled Carbon Nanotubes

The characterization of individual carbon nanotubes with Raman spectroscopy, especially by using different E_{laser} lines, includes many experimental challenges and strongly depends on the utilized Raman setup as well as on the sample preparation technique. We used the measurement strategy of preparing carbon nanotubes on a substrate and scanning huge surface areas with a sensitive fast-operating home-built Raman system described previously in detail, in Ref. 1. An additional

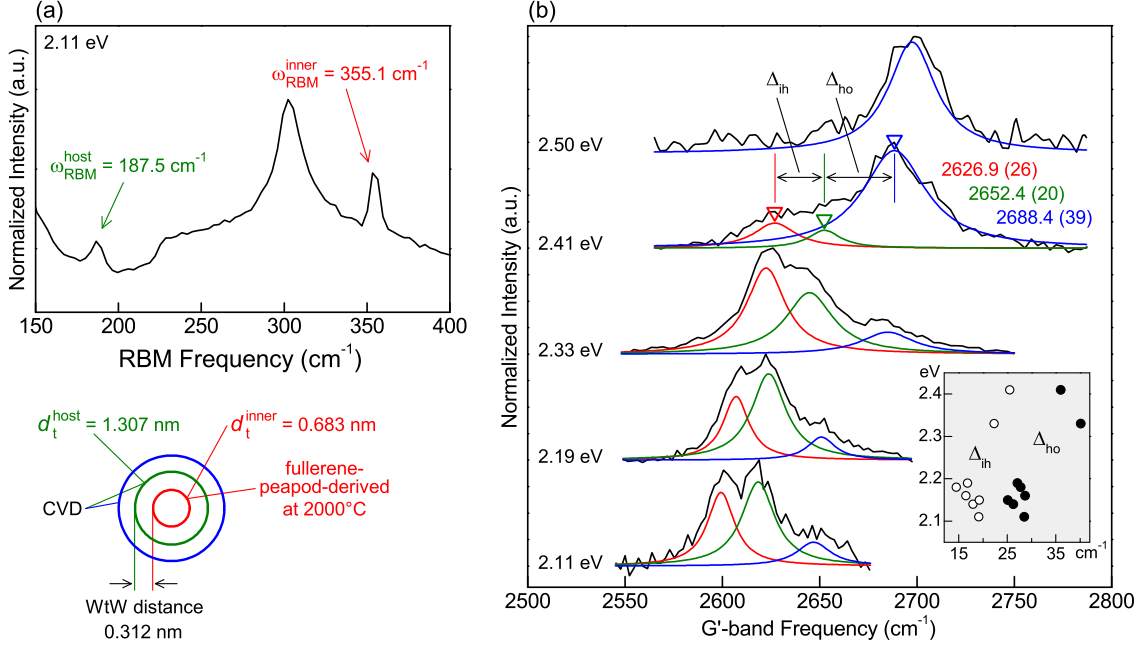


FIG. 4. The low Raman frequency range in (a) shows the resonant RBMs for the two inner nanotubes of an individual TWNT lying on a silicon Si/SiO₂ substrate (the Raman peak at 303 cm^{-1} is from the Si/SiO₂ substrate). Panel (b) depicts the G'-band spectra taken with five different laser lines in the high Raman frequency range of the individual TWNT shown in (a). Each Raman spectrum between E_{laser} values of 2.11 and 2.41 eV shows three well resolved G'-lines coming from the three concentric nanotubes. The inset in panel (b) depicts the G'-line separations Δ_{ih} (open circles) and Δ_{ho} (closed circles), where i, h and o refer to the inner, host, and outer nanotube. The Raman intensity of each G'-line change, and all G'-lines shift towards higher frequencies, as well as tend to increase the G'-peak widths by increasing E_{laser} , as indicated in the inset.

benefit of this measurement strategy is, that all Raman spectra of the individual species include the Raman response of the silicon substrate, which is well-known and can be used for calibration purposes, as well as for the identification of features with very weak resonant RBM signals. Moreover, the silicon substrate acts as a heat sink, so that relatively high laser power levels, as, for example, as high as 7 mW by a laser spot size of 1 μm , can be used. Our measurement strategy also allows an understanding of the complex carbon nanotube growth process, so that, for example, peapod-derived inner nanotubes with very small nanotube diameters can be synthesized and afterwards characterized in detail.

Figure 4(a) shows a spectrum with the RBMs for the inner and host nanotubes of an individual TWNT. These two inner nanotubes have the (6,4)@S flavor (or S@S) and with the knowledge of the two nanotube diameters, $d_t^{(6,4)} = 0.683 \text{ nm}$ and $d_t^{\text{host}} = 1.307 \text{ nm}$, respectively, we can accurately determine the WtW distance between the inner two nanotubes to be 0.312 nm. Figure 4(b) depicts the E_{laser} -dependent G'-band spectra of this individual TWNT. These spectra show that each of the concentric nanotubes contributes independently to the G'-band because of the observed triple-peak splitting. The triple-peak structures of the G'-band confirm that the intertube interactions of the TWNT system are weak.

The consequence of this weak interaction is that the electronic band structure of each concentric nanotube is independent and different from each other, which means that the concentric nanotubes are structurally incommensurate with each other. Beyond that, a multi-walled carbon nanotube system does not exhibit the same kind of band coupling as a multi-layer graphene system has. Moreover, curvature effects¹⁰ contribute to the triple-peak structure formation. By increasing the laser excitation energy, we observe that: (1) each of the three G'-lines upshift in frequency, (2) the Raman intensities change because different resonant windows are applicable for each of the three constituent nanotubes, (3) the fwhm line width of each G'-line as well as (4) the G'-line separations Δ_{ih} and Δ_{ho} (i = inner, h = host, and o = outer nanotube) tend to increase in that order. The latter behavior is highlighted in the inset of Fig. 4(b). We also see that the G'-peaks of the inner and host nanotubes, which are dominant from 2.11 to 2.33 eV, are still somewhat weaker at 2.41 eV and are too low in intensity to observe at $E_{\text{laser}} = 2.50 \text{ eV}$. This is in contrast to the increasing G'-peak intensity of the outer nanotube with increasing E_{laser} indicating that the RBM could be resonant in the high energy region $E_{\text{laser}} > 2.41 \text{ eV}$. We notice that the G'-peaks of the semiconducting inner nanotube and host nanotube show similar resonant windows, the outer nanotube also has an approximately

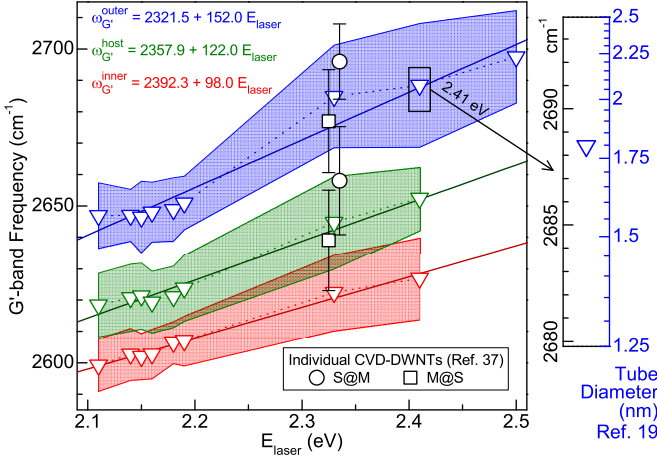


FIG. 5. The colored triangles and the error bars represent the positions and fwhm of the G'-lines for the inner (red color), host (green color) and outer nanotube (blue color) of an individual TWNT. The solid lines represent the G'-peak dispersions for each concentric nanotube. We also included the experimental G'-band results from two individual CVD DWNTs at 2.33 eV (see circle and square symbols).³⁷ The right panel depicts the Relation A (Table I) between $\omega_{G'}$ and d_t based on a Raman study on individual SWNTs measured at 2.41 eV.¹⁹

similar resonant window, but occurring in another E_{laser} region. The observations also point out that the G'-band resonant window is around 0.7 eV wide, assuming that the RBM and the G'-band resonant windows would be centered at the same value of E_{laser} . This is a reasonable assumption because we observe the RBMs and the G-band simultaneously (incident resonance). Kim *et al.*²⁵ reported that semiconducting nanotubes have wider resonant windows in comparison to metallic nanotubes, which allows us to speculate that the outer nanotube might be a semiconducting nanotube. Souza Filho *et al.*⁴⁴ reported a detailed G'-band analysis of individual semiconducting SWNTs, showing that a few SWNTs exhibit a splitting into two G'-lines due to the occasional occurrence of the resonance condition for two distinct transition energies at the same time, as, for example, the transitions E_{33}^S and E_{44}^S . Because of the observed G'-band resonant window information for the three concentric nanotubes in Fig. 4(b), we can exclude this anomalous two-peak splitting possibility for our TWNT system generally.

We plot in Fig. 5 the G'-line positions (triangles) and widths (depicted as error bars) of the three concentric nanotubes from the individual TWNT presented in Fig. 4(b). The three fitted linear G'-peak dispersions of the individual TWNT show an increasing $\partial\omega_{G'}/\partial E_{\text{laser}}$ dependence for each of the three concentric nanotubes with values of 98 (inner nanotube) < 122 (host nanotube) < 152 (outer nanotube) cm^{-1}/eV , as shown in the figure. Especially the $\partial\omega_{G'}/\partial E_{\text{laser}}$ slopes of the inner nanotube and host nanotube from the individual

TWNT are in accordance with the frequency dispersions of bundled DWNTs^{22,35}, which are also plotted in Fig. 3. We claim that the reason why the G'-peak dispersion decreases in going from the outer to the inner nanotube is due to the fact that nanotubes with smaller diameters exhibit larger curvature effects. This indicates a flattening of the dispersion as the K-point is approached. Interestingly, the slope of the outer nanotube, with a value of 152 cm^{-1}/eV , is relatively large and is 30 cm^{-1}/eV larger relative to the slope of the host nanotube. At this point it is important to remember that the host nanotube and the outer nanotube are grown simultaneously with the CVD method. This increase in slope is comparable with the increase in slope of 33 cm^{-1}/eV previously found for the inner and host nanotubes from bundled CVD DWNTs with slightly larger nanotube diameters as compared to fullerene-peapod-derived DWNTs.³⁷ Moreover, the Δ_{ih} distance is continuously smaller in contrast with Δ_{ho} , which are for example 22.3 and 40.1 cm^{-1} , respectively, at 2.33 eV (more details can be seen in the right panel from Fig. 4(b)). We also included in Fig. 5 the reported G' frequencies and widths from two individual CVD DWNTs.⁴⁵ These two individual DWNTs have two different flavors, respectively, S@M and M@S, and the Δ_{ih} distances in both cases are 38 cm^{-1} at 2.33 eV, which is comparable with the $\Delta_{\text{ho}} = 40.1 \text{ cm}^{-1}$ distance obtained from the individual TWNT, as it is expected to be. Otherwise, the G'-line positions of these individual species are quite different. The inset in Fig. 5 shows the experimental G'-peak position of the outer nanotube from the individual TWNT at $E_{\text{laser}} = 2.41 \text{ eV}$. Here, the right scale bar represents the nanotube diameters according to the relation $\omega_{G'} = 2708.1 - 35.4/d_t$ (Rela-

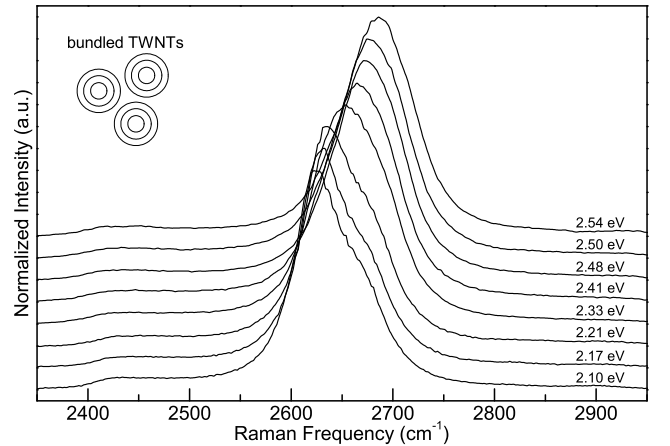


FIG. 6. The spectra show the G'-band of bundled TWNTs taken at E_{laser} between 2.10 and 2.54 eV from which we can extract important information about the lineshape differences as well as the laser energy dependencies. The G'-band spectrum together with the RBM intensities taken at 2.41 eV are shown in detail in Fig. 7.

tion A in Table I) found from the analysis for individual SWNTs with nanotube diameters between 1.25 and 2.5 nm.¹⁹ Through this relation, we can infer that the outer nanotube from the individual TWNT could have a diameter of approximately 1.797 nm, which results in a WtW distance between the middle and outer nanotube of 0.245 nm. This WtW distance is clearly smaller in comparison to the 0.335 nm interlayer distance of graphite.⁴⁶ We understand that this difference might be related to stronger interactions of the outer nanotube with the substrate when compared to that interaction of the outer nanotubes in a DWNT system. Nanotubes with larger diameter have more surface contact, which helps to establish a stronger nanotube-substrate interaction.

TABLE I. Details about the three $\omega_{G'}$ relations^{19,20} utilized in Fig. 5 and Fig. 7, with d_t obtained through the relation³² $\omega_{\text{RBM}} = 218.3/d_t + 15.9$.

Relation	$\omega_{G'} \text{ (cm}^{-1}\text{)}$	Ref.
A	$2708.1 - 35.4/d_t$	19
B	$(2645 - 30/d_t^2) + [(0.45 \text{ eV}) \times (103 \text{ cm}^{-1}/\text{eV})]$	20
C	$(2645 - 30/d_t^2) + [(0.45 \text{ eV}) \times (80 \text{ cm}^{-1}/\text{eV})]$	20

Figure 6 depicts the G' -band spectra of the bundled TWNTs taken at E_{laser} between 2.10 and 2.54 eV. The spectra in the E_{laser} range between 2.10 and 2.21 eV exhibit an asymmetric lineshape with a strong low frequency shoulder. These G' -band intensities correspond to the resonant condition of the (6,5) and (6,4) inner nanotubes of bundled TWNTs, which are strongly resonant with E_{laser} and show a high intensity in our sample.¹ A change in the spectra is observed when exciting with higher E_{laser} values: For example at 2.50 eV, the G' -band is more symmetric. The bundled TWNT results also underline the statements discussed above, where we have emphasized that nanotubes with small diameters as well as metallic nanotubes contribute strongly to the observed G' -band intensities. Moreover, it also confirms that the outer nanotubes will have a steeper dispersion compared to the inner and host nanotubes. In Fig. 6, one can easily observe that asymmetric peak at $E_{\text{laser}} = 2.10$ eV evolves to a more symmetric peak at higher E_{laser} .

The Raman spectra in Fig. 7 show in detail the G' -bands from bundled TWNTs and DWNTs taken at $E_{\text{laser}} = 2.41$ eV. The filled spectra represent the RBM intensities of the bundled TWNTs and DWNTs, but transformed into $\omega_{G'}$ using the three relations listed in Table I. Here, we used the ω_{RBM} vs. $\omega_{G'}$ relations with a $1/d_t^2$ dependence for the host nanotubes (Relation B)

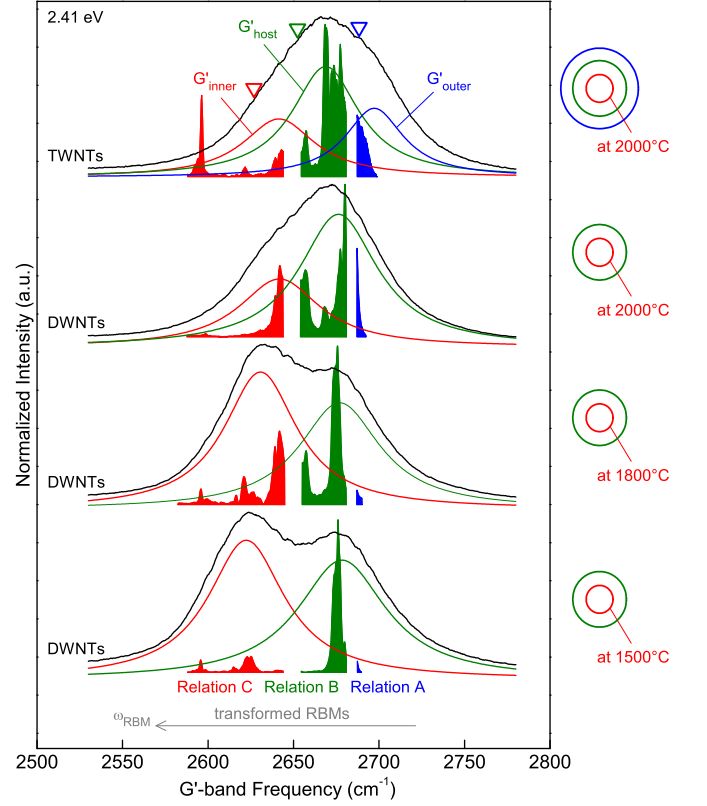


FIG. 7. The Raman spectra with the fitted Lorentzian lines show the G' -band results from bundled TWNTs and bundled DWNTs taken at 2.41 eV, where the inner nanotubes were fabricated by different annealing temperatures. The filled spectra indicate that the RBM intensities converted to the $\omega_{G'}$ values using three different ω_{RBM} vs. $\omega_{G'}$ relations^{19,20} for the inner, host, and outer nanotubes (in the case of the DWNTs: host nanotubes with large diameters). The details about the Relations A, B and C are given in Table I. These relations are separated at ω_{RBM} values of 144 and 258 cm^{-1} , which represent nanotube diameters that are larger (smaller) than 1.7 nm (0.9 nm), according to the relation³² $\omega_{\text{RBM}} = 218.3/d_t + 15.9$. The three triangles represent the G' -band frequencies from the individual TWNT shown in Fig. 4(b).

and for the inner nanotubes (Relation C) according to Ref. 20 since the curvature effect is expected to apply to the host nanotubes and even more strongly to the inner nanotubes. Because the outer nanotubes from bundled TWNTs and the host nanotubes from the bundled DWNTs with large diameters are expected in general to have weak curvature influences, we used the Relation A with a $1/d_t$ dependence for large diameter nanotubes.¹⁹ All the relations in Table I are distinguished by frequency-gaps between the calculated $\omega_{G'}$ values from the associated ω_{RBM} values of the respective concentric nanotubes on the basis of SWNTs. Nevertheless, we see relatively good agreement between the measured RBM intensities and the fitted G' -Lorentzian line shapes for the bundled DWNTs and TWNTs. We

observe that the G' -band from the bundled TWNTs is clearly distinguished by their additional G' intensities at higher frequencies, which belong to the resonant outer nanotubes with larger d_t . We also observe distinct correlations between the inner nanotubes of both FWNT systems. Here, the G' -band intensities of the inner nanotubes from the bundled DWNTs at 1500 and 1800 °C systematically occur at lower frequencies and with higher intensities in comparison to the bundled DWNTs and TWNTs at 2000 °C. The three peak structure of the G' -band from bundled TWNTs could be confirmed by including the G' peak positions (three triangles) from the individual TWNT at 2.41 eV shown in Fig. 4(b), which are, respectively, 2626.9, 2652.4, and 2688.4 cm^{-1} . Moreover, we can directly determine that the investigated individual TWNT is expected to be a relatively small diameter, compared to those in the bundled sample, which is also confirmed by TEM observations reported in Ref. 29.

IV. CONCLUSION

We analyzed in detail the spectral changes in frequency, width and intensity of the RBM and G' -band of peapod-derived bundled DWNTs by the stepwise modification of the annealing temperature between 1500 and 2000 °C. As a result, we could extract important information about the growth process, as for example, that higher annealing temperatures produce DWNTs with larger diameters, which is reflected in both the observations on the RBMs and the G' -band frequencies. Here, especially the G' -band frequency and intensity of

the inner nanotubes revealed a strong dependence on the nanotube diameter and metallicity. The results from the bundled DWNTs helped to make the analysis of the E_{laser} -dependent results from bundled TWNTs, where we discussed several relations between ω_{RBM} and $\omega_{G'}$ at 2.41 eV as observed experimentally. The observation of the G' -band from an individual TWNT taken at several laser excitation energies makes clear that each of the concentric nanotubes contributes independently from one another through their well-developed triple-peak structure; this is a clear indication of a weakly interacting system. Thereby, we obtain different dispersions for each nanotube showing increasing $\partial\omega_{G'}/\partial E_{\text{laser}}$ values, respectively, of $98 < 122 < 152 \text{ cm}^{-1}/\text{eV}$, for the inner, host, and outer nanotubes in the TWNT system. In addition, we analyzed the G' -band results from bundled TWNTs which confirmed the observed behavior suggested by the individual TWNT measured.

ACKNOWLEDGMENTS

M. S. D. and P. T. A. acknowledge the NSF-DMR 10-04147 grant. H. M. acknowledges support from the JSPS KAKENHI Grant Number 24710115. U. W. and E. P. acknowledge support by the German Excellence Initiative *via* the Nanosystems Initiative Munich (NIM). Y. A. K. acknowledges the support from Global Research Laboratory (2013056090) through the National Research Foundation of Korea (NRF) funded by the Ministry of Science, ICT (Information and Communication Technologies) and Future Planning.

-
- ¹ T. Ch. Hirschmann, P. T. Araujo, H. Muramatsu, X. Zhang, K. Nielsch, Y. A. Kim, and M. S. Dresselhaus, *ACS Nano* **7**, 2381–2387 (2013).
 - ² T. Ch. Hirschmann, P. T. Araujo, H. Muramatsu, J. F. Rodriguez-Nieva, M. Seifert, K. Nielsch, Y. A. Kim, and M. S. Dresselhaus, *ACS Nano* **8**, 1330–1341 (2014).
 - ³ A. Jorio, M. S. Dresselhaus, R. Saito, and G. Dresselhaus, *Wiley-VCH* (2011).
 - ⁴ R. A. Jishi, L. Venkataraman, M. S. Dresselhaus, and G. Dresselhaus, *Chem. Phys. Lett.* **77**, 209 (1993).
 - ⁵ H. Telg, J. G. Duque, P. T. Staiger, X. Tu, F. Hennrich, M. M. Kappes, M. Zheng, J. Maultzsch, C. Thomsen, and S. K. Doorn, *ACS Nano* **6**, 904–911 (2012).
 - ⁶ C. Thomsen and S. Reich, *Phys. Rev. Lett.* **85**, 5214–5217 (2000).
 - ⁷ V. Zólyomi and J. Kúrti, *Phys. Rev. B* **66**, 073418 (2002).
 - ⁸ V. Zólyomi, J. Kúrti, A. Grüneis, and H. Kuzmany, *Phys. Rev. Lett.* **90**, 157401 (2003).
 - ⁹ R. P. Vidano, D. B. Fischbach, L. J. Willis, and T. M. Loehr, *Solid State Commun.* **39**, 341 (1981).
 - ¹⁰ A. C. Ferrari, J. C. Meyer, V. Scardaci, C. Casiraghi, M. Lazzeri, F. Mauri, S. Piscanec, D. Jiang, K. S. Novoselov, S. Roth, and A. K. Geim, *Phys. Rev. Lett.* **97**, 187401 (2006).
 - ¹¹ C. H. Lui, Z. Li, Z. Chen, P. V. Klimov, L. E. Brus, and T. F. Heinz, *Nano Lett.* **11**, 164–169 (2011).
 - ¹² W. Fang, A. L. Hsu, R. Caudillo, Y. Song, A. G. Birdwell, E. Zakar, M. Kalbac, M. Dubey, T. Palacios, M. S. Dresselhaus, P. T. Araujo, and J. Kong, *Nano Lett.* **13**, 1541–1548 (2013).
 - ¹³ J. Kúrti, V. Zólyomi, A. Grüneis, and H. Kuzmany, *Phys. Rev. B* **65**, 165433 (2002).
 - ¹⁴ C. A. Cooper, and R. J. Young, *J. Raman Spectrosc.* **30**, 929–938 (1999).
 - ¹⁵ P. M. Ajayan, L. S. Schadler, C. Giannaris, and A. Rubio, *Adv. Mat.* **12**, 750–753 (2000).
 - ¹⁶ M. S. Amer, M. M. El-Ashry, and J. F. Maguire, *The Journal of Chem. Phys.* **121**, 2752 (2004).
 - ¹⁷ M. A. Pimenta, E. B. Hanlon, A. Marucci, P. Corio, S. D. M. Brown, S. A. Empedocles, M. G. Bawendi, G. Dresselhaus, and M. S. Dresselhaus, *Brazilian Journal of Phys.* **30**, 423–427 (2000).
 - ¹⁸ M. S. Dresselhaus, G. Dresselhaus, A. Jorio, A. G. Souza Filho, and R. Saito, *Carbon* **40**, 2043–2061 (2002).

- ¹⁹ A. G. Souza Filho, A. Jorio, G. G. Samsonidze, G. Dresselhaus, M. A. Pimenta, M. S. Dresselhaus, A. K. Swan, M. S. Ünlü, B. B. Goldberg, and R. Saito, *Phys. Rev. B* **67**, 035427 (2003).
- ²⁰ J. F. Cardenas, *Chem. Phys. Lett.* **430**, 367–369 (2006).
- ²¹ I. O. Maciel, M. A. Pimenta, M. Terrones, H. Terrones, J. Campos-Delgado, and A. Jorio, *Phys. Status Solidi B* **245**, 2197–2200 (2008).
- ²² R. Pfeiffer, H. Kuzmany, F. Simon, S. N. Bokova, and E. Obraztsova, *Phys. Rev. B* **71**, 155409 (2005).
- ²³ K. Papagelis, J. Arvanitidis, D. Christofilos, K. S. Andrikopoulos, T. Takenobu, Y. Iwasa, H. Kataura, S. Ves, and G. A. Kourouklis, *Phys. Status Solidi B* **244**, 116–120 (2007).
- ²⁴ R. S. Alencar, A. L. Aguiar, A. R. Paschoal, P. T. C. Freire, Y. A. Kim, H. Muramatsu, M. Endo, H. Terrones, M. Terrones, A. San-Miguel, M. S. Dresselhaus, and A. G. Souza Filho *J. Phys. Chem. C* **118**, 8153–8158 (2014).
- ²⁵ K. K. Kim, J. S. Park, S. J. Kim, H. Z. Geng, K. H. An, C.-M. Yang, K. Saito, R. Saito, and Y. H. Lee, *Phys. Rev. B* **76**, 205426 (2007).
- ²⁶ L. X. Benedict, V. H. Crespi, S. G. Louie, and M. L. Cohen, *Phys. Rev. B* **52**, 14935–14940 (1995).
- ²⁷ F. Simon, V. Zolyomi, R. Pfeiffer, H. Kuzmany, J. Koltai, and J. Kürti, *Phys. Rev. B* **81**, 125434 (2010).
- ²⁸ H. Muramatsu, T. Hayashi, Y. A. Kim, D. Shimamoto, M. Endo, V. Meunier, B. G. Sumpter, M. Terrones, and M. S. Dresselhaus, *Small* **5**, 2678–2682 (2009).
- ²⁹ H. Muramatsu, D. Shimamoto, T. Hayashi, Y. A. Kim, M. Terrones, M. Endo, and M. S. Dresselhaus, *Adv. Mater.* **23**, 1761–1764 (2011).
- ³⁰ B. W. Smith, M. Monthieux, and D. E. Luzzi, *Nature* **396**, 323 (1998).
- ³¹ E. Hernandez, V. Meunier, B. W. Smith, R. Rurli, H. Terrones, M. Buongiorno Nardelli, M. Terrones, D. E. Luzzi, and J.-C. Charlier, *Nano Lett.* **3**, 1037–1042 (2003).
- ³² M. Endo, Y. A. Kim, T. Hayashi, H. Muramatsu, M. Terrones, R. Saito, F. Villalpando-Paez, S. G. Chou, and M. S. Dresselhaus, *Small* **2**, 1031–1036 (2006).
- ³³ P. T. Araujo, I. O. Maciel, P. B. C. Pesce, M. A. Pimenta, S. K. Doorn, H. Qian, A. Hartschuh, M. Steiner, L. Grigorian, K. Hata, and A. Jorio, *Phys. Rev. B* **77**, 241403R (2008).
- ³⁴ R. Pfeiffer, F. Simon, H. Kuzmany, and V. N. Popov, *Phys. Rev. B* **72**, 161404 (2005).
- ³⁵ M. Kalbac, L. Kavan, M. Zukalova, and L. Dunsch, *Carbon* **42**, 2915–2920 (2004).
- ³⁶ G. M. do Nascimento, T. Hou, Y. A. Kim, H. Muramatsu, T. Hayashi, M. Endo, N. Akuzawa, and M. S. Dresselhaus, *Nano Lett.* **8**, 4168–4172 (2008).
- ³⁷ F. Villalpando-Paez, L. G. Moura, C. Fantini, H. Muramatsu, T. Hayashi, Y. A. Kim, M. Endo, M. Terrones, M. A. Pimenta, and M. S. Dresselhaus, *Phys. Rev. B* **82**, 155416 (2010).
- ³⁸ G. M. do Nascimento, T. Hou, Y. A. Kim, H. Muramatsu, T. Hayashi, M. Endo, N. Akuzawa, and M. S. Dresselhaus, *Carbon* **49**, 3585–3596 (2011).
- ³⁹ X. Liu, H. Kuzmany, T. Saito, and T. Pichler, *Phys. Status Solidi B* **248**, 2492–2495 (2011).
- ⁴⁰ M. Terrones, H. Terrones, F. Banhart, J.-C. Charlier, and P. M. Ajayan, *Science* **288**, 1226–1229 (2000).
- ⁴¹ M. Endo, T. Hayashi, H. Muramatsu, Y. A. Kim, H. Terrones, M. Terrones, and M. S. Dresselhaus, *Nano Lett.* **4**, 1451–1454 (2004).
- ⁴² H. Muramatsu, T. Hayashi, K. Fujisawa, T. Tojo, Y.-I. Ko, A. Morelos-Gomez, K.-S. Yang, Y. A. Kim, M. Endo, M. Terrones, and M. S. Dresselhaus, *RSC Adv.* **3**, 26266 (2013).
- ⁴³ Sihan Zhao, Yasumitsu Miyata, Hisanori Shinohara, and Ryo Kitaura, *Carbon* **71**, 159–165 (2014).
- ⁴⁴ A. G. Souza Filho, A. Jorio, A. K. Swan, M. S. Ünlü, B. B. Goldberg, R. Saito, J. H. Hafner, C. M. Lieber, M. A. Pimenta, G. Dresselhaus, and M. S. Dresselhaus, *Phys. Rev. B* **65**, 085417 (2002).
- ⁴⁵ F. Villalpando-Paez, H. Son, D. Nezich, Y. P. Hsieh, J. Kong, Y. A. Kim, D. Shimamoto, H. Muramatsu, T. Hayashi, M. Endo, M. Terrones, and M. S. Dresselhaus, *Nano Lett.* **8**, 3879–3886 (2008).
- ⁴⁶ R. Bacon, *J. Appl. Phys.* **31**, 283–290 (1960).